Coherent Optical Phase-Derived Ranging With High Sensitivity and Accuracy

Lihan Wang, Xiangchuan Wang, Shupeng Li, and Shilong Pan, *Fellow, IEEE*

***Abstract*—Optical transfer delay (OTD) measurement enables the high performance of distributed coherent radar and optically controlled phase arrays. However, achieving high-accuracy and large-range OTD measurement in photonic integrated chips, outdoor free-space optics, and optical links with significant insertion loss is challenging. This article proposes a coherent optical phase-derived ranging (PDR) system to enhance the OTD measurement sensitivity. In the experiments, the stability of the coherent system was improved 35 times compared to the incoherent system when measuring an optical device with an insertion loss of 30 dB. The sensitivity of the proposed system reaches −80 dBm, which is 46 dB better than the commercial PDR-based product. In addition, the error introduced by the Doppler effect was eliminated with the proposed demodulation method, enabling OTD measurement of a variable optical link.**

***Index Terms*—Coherent demodulation, coherent detection, optical transfer delay measurement, phase-derived ranging.**

I. Introduction

ACCURATE measurement and controlling of optical transfer delay (OTD) play a crucial role in microwave photonics and optical communications [1], [2], [3], [4], [5] for optical buffering, beamforming, clock synchronization, etc. With the rapid development of photonic integrated chips, integrated optical delay lines (ODLs) have been developed [6], [7], [8], [9], which are always associated with large insertion loss and therefore challenge the OTD measurement sensitivity. For example, the average propagation loss of the silicon waveguide is 3 dB/cm, 10^6 times that of the optical fibers. The insertion loss of the integrated ODLs is directly related to the amount of delay. In [8], a delay of 5 ns corresponds to an insertion loss of above 28 dB. Therefore, achieving high sensitivity and a large measurement range is necessary for the ODL measurement. On the other hand, in outdoor free-space optics, severe weather would induce high attenuation of up to 480 dB/km. Even if ignoring the weather element, the reflectivity of the detected object may be very low in some circumstances. All these applications require high sensitivity OTD measurement system.

Phase-derived ranging (PDR) [10] is one of the most effective methods for OTD measurement owing to its incomparable high accuracy and large measurement range. In a PDR system, the OTD will be transferred into the phase variation of the modulated signal, which can be detected with high accuracy in the electrical domain. However, the traditional PDR system has limited measurement sensitivity. If we measure an optical device or optical link with a large insertion loss, the optical carrier would be suppressed accordingly, so the signal-to-noise ratio (SNR) of the OTD measurement system would deteriorate severely. To overcome this problem, one can apply an avalanche photodiode (APD), of which the current gain is 100 times larger than a PIN photodiode. However, the phase of the APD output signal is closely related to the intensity of the optical signal, which inevitably introduces large OTD measurement errors [11].

Generally, coherent detection has better-receiving sensitivity than incoherent detection due to the gain provided by the reference signal. However, to the best of our knowledge, no coherent PDR-based OTD measurement methods have been reported. This is because the reference laser's phase noise would severely degrade the measurement accuracy of the PDR. One solution to eliminate the phase noise is to use variable optical delay lines to match the length of the reference path and measurement path [12]. In the PDR, however, the optical length of the optical link under test (OLUT) is unknown, making the precise length matching in the reference path unreliable. Moreover, the reference optical delay line is susceptible to environmental disturbance, which produces additional measurement errors. An optical phase lock loop (OPLL) can also compensate for the laser phase noise [13], [14], in which the phase of the beat photocurrent between the signal light and local oscillator (LO) laser is first extracted, and then the phase error is used to modulate the LO laser in real-time. However, this approach requires a short feedback loop to track the phase noise. In addition, the OPLL is easy to lose lock when measuring a variable OLUT.

In addition, coherent optical PDR would be affected by the Doppler effect. The Doppler effect results in a frequency offset between the LO signal and the probe signal, which affects the accuracy of phase detection. To reduce the impacts of the Doppler effect on phase detection, one approach is using a quadrature demodulator [15], [16], [17] to separate the doppler component and the phase of the probe signal, which increases the system complexity. Recently, some phase-coded-based light detection and

Manuscript received 20 May 2023; revised 31 August 2023; accepted 8 September 2023. Date of publication 12 September 2023; date of current version 16 January 2024. This work was supported in part by the National Natural Science Foundation of China under Grants 62271249 and 62075095 and in part by the Key Research and Development Program of Jiangsu Province under Grant BE2020030. *(Corresponding authors: Xiangchuan Wang; Shilong Pan.)*

Lihan Wang, Xiangchuan Wang, and Shilong Pan are with the National Key Laboratory of Microwave Photonics, Nanjing University of Aeronautics and Astronautics, Nanjing 210016, China (e-mail: andwwlh@nuaa.edu.cn; wangxch@nuaa.edu.cn; pans@nuaa.edu.cn).

Shupeng Li is with Suzhou LiuYaoSi Information Technologies Company, Ltd., Suzhou 215500, China (e-mail: lsp@newkeytech.com).

Color versions of one or more figures in this article are available at https://doi.org/10.1109/JLT.2023.3314523.

Digital Object Identifier 10.1109/JLT.2023.3314523

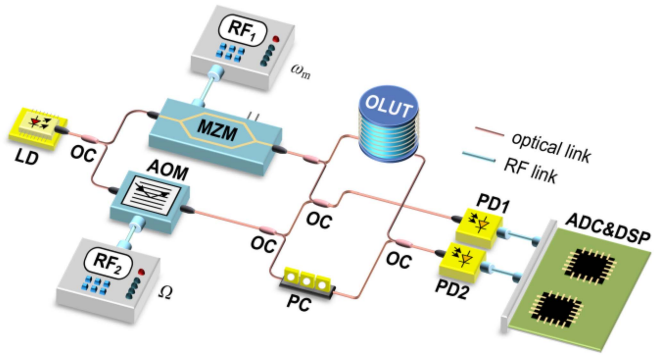

Fig. 1. Schematic diagram of the proposed OTD measurement system based on coherent detection. LD, laser diode. MZM, Mach–Zehnder modulator. AOM, acousto-optic modulator. RF, radio frequency. OLUT, the optical link under test. PD, photodetector. ADC, analog-to-digital convertor. DSP, digital signal processor.

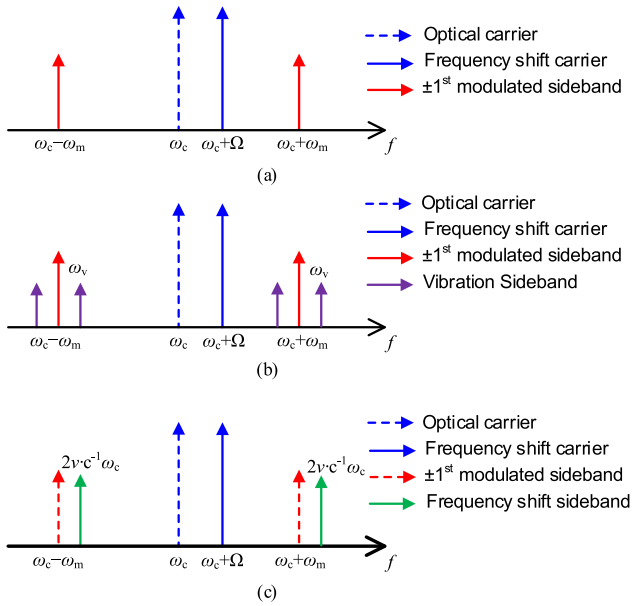

Fig. 2. Optical spectrum of the combined signal in different measurement scenes. (a) Static measurement. (b) LiDAR system. (c) Vibration sensor.

ranging (LiDAR) systems proposed the time-multiplexing [18] method and frequency-multiplexing [19] methods to remove the doppler frequency shift. The essence of these technologies is to accurately measure the doppler frequency and then compensate the frequency offset to the detected phase. It consumes additional time and frequency resources of the ranging system. Moreover, the computational complexity of these approaches can also be high.

In this article, we introduce a coherent optical PDR method, which can improve the measurement sensitivity and is suitable for measuring variable OLUTs. In the coherent detection system, the probe signal is a carrier-suppressed double-sideband signal, while the LO signal has a small frequency difference from the optical carrier. The beat photocurrent between the LO signal and the probe signal contains two frequency components, which carry the inverse phase error and the same OTD information. Therefore, in the coherent demodulation process, the laser phase noise and doppler error can be removed simultaneously in the digital domain while keeping the OTD information unchanged. In the experiment, benefitting from the coherent detection, the system stability enhanced 35 times compared to the incoherent PDR system when the system insertion loss is 30 dB. The measurement sensitivity of the system reaches at least −80 dBm. The dynamic measurement ability in our system was also successfully verified.

II. Guidelines for Manuscript Preparation

A. Static Measurement

Fig. 1 shows the schematic of the proposed coherent OTD measurement system. The optical carrier with a frequency of ω_c launched from the laser diode (LD) is divided into two branches by an optical coupler (OC). In one branch, the optical signal is modulated by an ω_m RF signal at an electro-optic modulator (EOM), which generates a carrier-suppressed double-sideband (CS-DSB) signal $E_m(t)$. Mathematically, the optical signal in the upper branch can be expressed as:

$$E_m(t) = [A_{-1}\exp j(-\omega_m t) + A_{+1}\exp j(\omega_m t)] \cdot \exp j[\omega_c t + \varphi(t)] \quad (1)$$

where $A_{\pm1}$ is the amplitude of the ±1st-order sideband of the modulated signal; $\varphi(t)$ is the time-varying phase fluctuation of the optical carrier induced by the laser phase noise.

The optical signal in the other branch (denoted as $E_s(t)$) goes through frequency shifting (FS) with a frequency of Ω by an acoustic optical modulator (AOM), which can be written as:

$$E_s(t) = A_s \exp(j[(\omega_c + \Omega)(t - \tau_0) + \varphi(t - \tau_0)]) \quad (2)$$

where τ_0 is the fixed delay between the two branches, A_s is the amplitude of the FS signal. Two driven signals on the different modulators are phase-locked to the same reference source.

In order to achieve coherent detection and demodulation, the CS-DSB signal is applied as the probe signal, while the FS signal is used as the LO signal. There are two portions in the system, including the measurement portion and the reference portion. In the measurement portion, the probe signal is injected into OLUT while the state-of-polarization (SOP) of LO signal is controlled by a polarization controller (PC) to maximize the output power of the coherent detection. For a large-range OTD measurement, the SOP of the probe signal could not be stable because of the impact of the surrounding environment. To avoid polarization fading, some polarization diversity techniques can be applied. Photodetector (PD1) receives the combination of the probe signal and LO signal. The optical spectrum of the combined signal is shown in Fig. 2(a). The photocurrent includes the beat frequency components $(\omega_m + \Omega)$ and $(\omega_m - \Omega)$. The photocurrent of the measurement portion without a DC component can be described as:

$$i_{PD1}(t) = \frac{\sqrt{2}}{2}\eta\alpha A_s\{A_{-1}\exp j[(\omega_m + \Omega)t + (\omega_c - \omega_m)\tau - (\omega_c + \Omega)\tau_0 + \varphi(t - \tau_0) - \varphi(t - \tau)]$$

$$+ A_{+1} \exp j \left[\left(\omega_{\mathrm{m}} - \Omega \right) t - \left(\omega_{\mathrm{c}} + \omega_{\mathrm{m}} \right) \tau + \left(\omega_{\mathrm{c}} + \Omega \right) \tau_0 - \varphi \left(t - \tau_0 \right) + \varphi \left(t - \tau \right) \right] \} \quad (3)$$

where η is the responsivity of PD, α is the insertion loss of the OLUT, and τ is the OTD under test. Similarly, in the reference portion, the probe signal is directly combined with LO signal without passing through the OLUT. Then, the combined signal enters into PD_2. The mathematic expression of the reference portion photocurrent is:

$$i_{\mathrm{PD2}} \left(t \right) = \frac{\sqrt{2}}{2} \eta A_{\mathrm{s}} \{ A_{-1} \exp j \left[\left(\omega_{\mathrm{m}} + \Omega \right) t - \left(\Omega + \omega_{\mathrm{c}} \right) \tau_0 + \varphi \left(t - \tau_0 \right) - \varphi \left(t \right) \right] + A_{+1} \exp j \left[\left(\omega_{\mathrm{m}} - \Omega \right) t + \left(\Omega + \omega_{\mathrm{c}} \right) \tau_0 - \varphi \left(t - \tau_0 \right) + \varphi \left(t \right) \right] \} \quad (4)$$

Two-port ADC acquires the two photocurrents simultaneously. By applying the fast Fourier Transform (FFT) algorithm, we can obtain the phases of the corresponding frequencies:

$$\Phi_{\mathrm{mea}} \left(\omega_{\mathrm{m}} + \Omega \right) = \left(\omega_{\mathrm{m}} + \Omega \right) t + \left(\omega_{\mathrm{c}} - \omega_{\mathrm{m}} \right) \tau - \left(\omega_{\mathrm{c}} + \Omega \right) \tau_0 + \varphi \left(t - \tau_0 \right) - \varphi \left(t - \tau \right) + 2 N_1 \pi \quad (5)$$

$$\Phi_{\mathrm{mea}} \left(\omega_{\mathrm{m}} - \Omega \right) = \left(\omega_{\mathrm{m}} - \Omega \right) t - \left(\omega_{\mathrm{c}} + \omega_{\mathrm{m}} \right) \tau + \left(\omega_{\mathrm{c}} + \Omega \right) \tau_0 - \varphi \left(t - \tau_0 \right) + \varphi \left(t - \tau \right) + 2 N_2 \pi \quad (6)$$

$$\Phi_{\mathrm{ref}} \left(\omega_{\mathrm{m}} + \Omega \right) = \left(\omega_{\mathrm{m}} + \Omega \right) t - \left(\omega_{\mathrm{c}} + \Omega \right) \tau_0 + \varphi \left(t - \tau_0 \right) - \varphi \left(t \right) + 2 N_3 \pi \quad (7)$$

$$\Phi_{\mathrm{ref}} \left(\omega_{\mathrm{m}} - \Omega \right) = \left(\omega_{\mathrm{m}} - \Omega \right) t + \left(\omega_{\mathrm{c}} + \Omega \right) \tau_0 - \varphi \left(t - \tau_0 \right) + \varphi \left(t \right) + 2 N_4 \pi \quad (8)$$

where $\Phi_{\mathrm{mea}}(\omega)$ and $\Phi_{\mathrm{ref}}(\omega)$ represent the phase discrimination results of the measurement and reference portion photocurrent, N_1 to N_4 are the unknown integers induced by the phase detector to restrict the detected phase has a limited range of 2π.

A phase interference cancellation method is proposed to achieve accurate OTD measurement. The first step is to obtain the phase difference induced by the measurement portion:

$$\Phi \left(\omega_{\mathrm{m}} + \Omega \right) = \Phi_{\mathrm{mea}} \left(\omega_m + \Omega \right) - \Phi_{\mathrm{ref}} \left(\omega_m + \Omega \right) = \left(\omega_{\mathrm{c}} - \omega_{\mathrm{m}} \right) \tau + \varphi \left(t \right) - \varphi \left(t - \tau \right) + 2 \left(N_1 - N_3 \right) \pi \quad (9)$$

$$\Phi \left(\omega_{\mathrm{m}} - \Omega \right) = \Phi_{\mathrm{mea}} \left(\omega_{\mathrm{m}} - \Omega \right) - \Phi_{\mathrm{ref}} \left(\omega_{\mathrm{m}} - \Omega \right) = \left(-\omega_{\mathrm{c}} - \omega_{\mathrm{m}} \right) \tau - \varphi \left(t \right) + \varphi \left(t - \tau \right) + 2 \left(N_2 - N_4 \right) \pi \quad (10)$$

It can be seen from (9) and (10), the phase difference of the two frequencies contains a common mode phase interference part: $\varphi(t)$– $\varphi(t–\tau) + \omega_{\mathrm{c}}\tau$. Thus, phase error in the common part can be compensated by the difference calculation:

$$\Phi \left(\omega_{\mathrm{m}} - \Omega \right) + \Phi \left(\omega_{\mathrm{m}} + \Omega \right) = -2 \omega_{\mathrm{m}} \tau + 2 \left(N_1 + N_2 - N_3 - N_4 \right) \pi \quad (11)$$

Finally, an extra phase unwrapping algorithm is performed to remove the integer ambiguity term (i.e., $2(N_1 + N_2 – N_3 – N_4)\cdot\pi$) in (11). Considering that the ambiguity term in (11) is an integer multiple of 2π, we can apply the modulus operator to rewrite (11):

$$\left[\Phi \left(\omega_{\mathrm{m}} - \Omega \right) + \Phi \left(\omega_{\mathrm{m}} + \Omega \right) \right]_{2\pi} = \left[-2 \omega_{\mathrm{m}} \tau \right]_{2\pi} = - 2 \omega_{\mathrm{m}} \tau + 2 k_{\mathrm{m}} \pi \quad (12)$$

where the symbol $[x]_y$ represents the modulo operator (x *mod* y), and k_{m} is a non-negative integer to keep $-2\omega_{\mathrm{m}}\tau$ limited from 0 to 2π. It should be noticed that the integer k_{m} is only determined by the frequency ω_{m} and OTD τ. Therefore, the calculation of the integer k_{m} can be regarded as a traditional phase unwrapping problem. It can be solved by sweeping the frequency ω_{m} [10]. The choice of the sweeping frequency is determined by the accuracy of the phase detector and the measurement range. After the phase unwrapping process, the OTD can be given by:

$$\tau = \frac{-\left[\Phi \left(\omega_{\mathrm{m}} - \Omega \right) + \Phi \left(\omega_{\mathrm{m}} + \Omega \right) \right]_{2\pi} + 2 k_{\mathrm{m}} \pi}{2 \omega_{\mathrm{m}}} \quad (13)$$

In order to ensure that there is no measurement dead zone, a self-calibration should be performed to remove the system length.

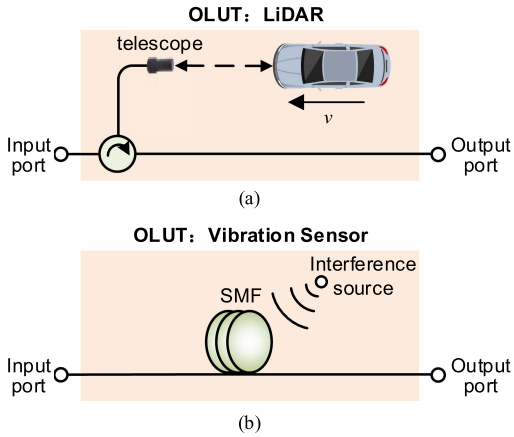

Fig. 3. Typical dynamic measurement scenes. (a) LiDAR system. (b) Vibration Sensor.

B. Dynamic Measurement

In the incoherent-based OTD measurement system, the system is immune from dynamic measurement as the doppler frequency shift is eliminated in the process of photoelectric conversion. However, these frequency components induced by the Doppler effect would affect the coherent system severely because the LO portion does not shift with the doppler frequency. In the following analysis, two OTD measurement application scenes, LiDAR and vibration sensors, are considered.

In the LiDAR system, as presented in Fig. 3(a), the optical signal from the measurement portion is frequency-shifted owing to the Doppler effect. The doppler frequency ω_{d} is approximately $2v\omega_{\mathrm{c}}/c$ in the reflection measurement, where v is the velocity of the measured object and c is the velocity of light. Accordingly, the phase detector can obtain the phase difference $\Phi(\omega_{\mathrm{m}}+\Omega–\omega_{\mathrm{d}})$ and $\Phi(\omega_{\mathrm{m}}–\Omega+\omega_{\mathrm{d}})$. In this case, (9) and (10) are rewritten as:

$$\begin{aligned}\Phi\left(\omega_{\mathrm{m}}+\Omega-\omega_{\mathrm{d}}\right) &= \Phi_{\mathrm{mea}}\left(\omega_m+\Omega-\omega_{\mathrm{d}}\right)-\Phi_{\mathrm{ref}}\left(\omega_m+\Omega\right)\\ &= -\omega_{\mathrm{d}}t+2\left(\omega_{\mathrm{c}}-\omega_{\mathrm{m}}+\omega_{\mathrm{d}}\right)\tau\\ &\quad+\varphi\left(t\right)-\varphi\left(t-2\tau\right)+2\left(N_1-N_3\right)\pi\end{aligned} \tag{14}$$

$$\begin{aligned}\Phi\left(\omega_{\mathrm{m}}-\Omega+\omega_{\mathrm{d}}\right) &= \Phi_{\mathrm{mea}}\left(\omega_{\mathrm{m}}-\Omega+\omega_{\mathrm{d}}\right)-\Phi_{\mathrm{ref}}\left(\omega_{\mathrm{m}}-\Omega\right)\\ &= \omega_{\mathrm{d}}t+2\left(-\omega_{\mathrm{c}}-\omega_{\mathrm{m}}-\omega_{\mathrm{d}}\right)\tau\\ &\quad-\varphi\left(t\right)+\varphi\left(t-2\tau\right)+2\left(N_2-N_4\right)\pi\end{aligned} \tag{15}$$

It can be observed from (14) and (15) that the phase difference between the two frequencies contains a common mode phase interference part: $-\omega_{\mathrm{d}}\cdot t+\varphi(t)–\varphi(t–2\tau)+2(\omega_{\mathrm{c}}+\omega_{\mathrm{d}})\tau$. Therefore, phase noise and the Doppler effect within this common part can be compensated by the difference calculation. Finally, the OTD can be given by:

$$\tau_{\mathrm{LiDAR}}=\frac{-\left[\Phi\left(\omega_{\mathrm{m}}-\Omega+\omega_{\mathrm{d}}\right)+\Phi\left(\omega_{\mathrm{m}}+\Omega-\omega_{\mathrm{d}}\right)\right]_{2\pi}+2k_{\mathrm{m}}\pi}{4\omega_{\mathrm{m}}} \tag{16}$$

From (16), we can eliminate the effect of the Doppler effect in OTD measurement. Although ω_{d} is an unknown component, it does not affect the digital phase detector to extract the accurate phase. By taking the FFT of the collected signal, we can obtain the FFT spectra. The two peaks in the spectra correspond to the frequency components $\omega_{\mathrm{m}}–\Omega+\omega_{\mathrm{d}}$ and $\omega_{\mathrm{m}}+\Omega–\omega_{\mathrm{d}}$. In PD_1, the argument of the complex numbers at these frequencies represents $\Phi_{\mathrm{mea}}(\omega_{\mathrm{m}}+\Omega–\omega_{\mathrm{d}})$ and $\Phi_{\mathrm{mea}}(\omega_{\mathrm{m}}–\Omega+\omega_{\mathrm{d}})$, respectively. The proposed elimination method is similar to the Frequency-Modulated Continuous-Wave (FMCW) ranging, which employs up-chirp and down-chirp signals. However, the fundamental issues addressed by these two methods are different. The FMCW ranging has the advantage of simultaneously obtaining both velocity and range information. In the proposed coherent PDR system, the primary object is to precisely measure the OTD while mitigating the impact of Doppler effects.

In a vibration sensor system, the vibration acting on an optical fiber, causing periodic changes in refractive index, is equivalent to optical phase modulation. Thus, the optical signal in the measurement portion can be written as:

$$\begin{aligned}E_{\mathrm{m\_vib}}\left(t\right) &= \left[A_{-1}\exp j\left(-\omega_{\mathrm{m}}t\right)+A_{+1}\exp j\left(\omega_{\mathrm{m}}t\right)\right]\\ &\quad\cdot\exp j\left[\omega_{\mathrm{c}}t+\varphi\left(t\right)+\delta\sin\left(\omega_{\mathrm{v}}t\right)\right]\\ &\approx \sum_{k=0}^{\infty}J_k\left(\delta\right)\cdot\left[A_{-k}\exp j\left(k\omega_{\mathrm{v}}-\omega_{\mathrm{m}}\right)t\right.\\ &\quad\left.+A_{+k}\exp j\left(k\omega_{\mathrm{v}}+\omega_{\mathrm{m}}\right)t\right]\end{aligned} \tag{17}$$

where δ is the vibration amplitude, ω_{v} is the vibration frequency, and J_k is k^{th} order Bessel functions of the first kind. The optical spectrum is given in Fig. 3(b). The OTD measurement under vibration is equivalent to static OTD measurement if the vibration component is filtered out by the IF filter, which is:

$$\tau_{\mathrm{vib}}=\frac{-\left[\Phi\left(\omega_{\mathrm{m}}-\Omega\right)+\Phi\left(\omega_{\mathrm{m}}+\Omega\right)\right]_{2\pi}+2k_{\mathrm{m}}\pi}{2\omega_{\mathrm{m}}} \tag{18}$$

When the vibration frequency is lower than 10 times the IF filter bandwidth, which is the reciprocal of the window function width, the vibration will degrade to linear motion cases. If the vibration frequency is slightly lower than the IF filter bandwidth, the phase detection accuracy will deteriorate significantly.

Obviously, (13), (16), and (18) have the same form. It means static measurement and dynamic measurement can adopt the same demodulation method. From the above analysis, the proposed coherent optical PDR system eliminates the impact of the Doppler effect without using any additional designs of hardware or algorithms.

III. Experiment and Discussion

In the experiments, a verification measurement system is constructed based on the configuration in Fig. 1. A laser (TeraXion, PS-TNL) with 1 kHz linewidth is applied to generate a continuous optical carrier which is divided into two branches. One branch is modulated at an MZM (IXBlue, MX-LN-40) to obtain a CS-ODSB signal. The RF_1 signal (R&SSMB100A) has a tunable range from 10 MHz to 31.8 GHz. The other branch is frequency-shifted at an AOM (Gooch&Housego Inc.) with a frequency of 200 MHz. After transmitting through the measurement and reference portion, two optical signals are converted into photocurrents at two PDs (CONQUER, KG-PD-10G). The photocurrent is amplified by a low noise amplifier (LNA, Connphy, CLN-1G18G-3025-S). An 8-bit oscilloscope (Tektronix DSA72004B) with a sampling rate of 12.5 GSa/s is applied to obtain the photocurrents.

A. Process of Coherent Demodulation

The coherent demodulation contains the following steps. Firstly, the waveforms amplified by two LNAs are collected by a dual-port oscilloscope. Then an FFT algorithm is performed to acquire the frequency response of the two waveforms. We have set RF_1 at 3 GHz so that the beat frequency components are 2.8 GHz and 3.2 GHz according to (3) and (4). The FFT spectra are shown in Fig. 4 with a rectangle window function width of 40 μs. Then the phase detection process can be accomplished by extracting the argument of the complex number. Fig. 5(a) and (b) present the result of phase detection from 2.8 GHz and 3.2 GHz over 120 s. Next, we compensate the common mode phase interference with difference calculation, as shown in Fig. 5(c). Finally, Fig. 5(d) removed the phase jump induced by the integer ambiguity with the remainder operation. With a 3 GHz modulation frequency, the phase fluctuation of 0.25° in Fig. 5(d) indicates an OTD ripple of 0.11 ps by taking (13). From the above demodulation process, the traditional technology cannot be simply applied in coherent PDR. This is because

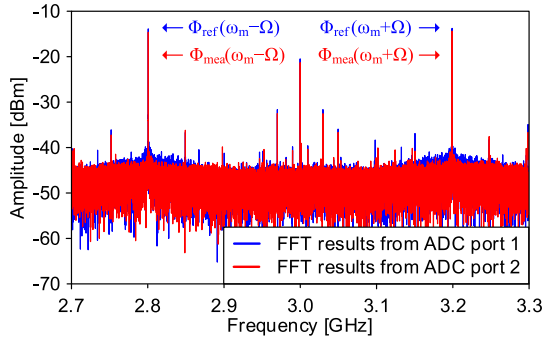

Fig. 4. The FFT spectra of the photocurrent from 2.7 GHz and 3.3 GHz with a rectangle window function width of 40 μs.

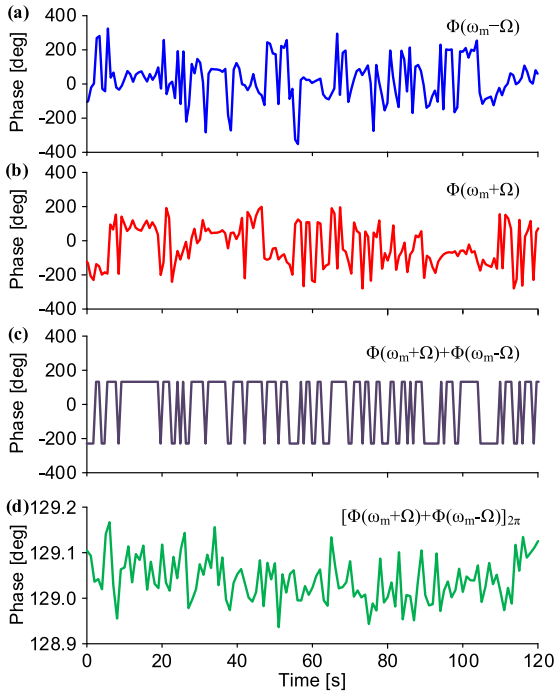

Fig. 5. Results of phase detection by the FFT algorithm over 120 seconds. (a) Photocurrent component of 2.8 GHz. (b) Photocurrent component of 3.2 GHz. (c) Measured phase after phase variation compensation. (d) Measured phase without phase jump.

the traditional PDR only employs the phase-detecting data from Fig. 5(a) or (b). However, Fig. 5(a) and (b) mix the laser phase noise and OTD information, providing no useful information for OTD measurement. To broaden the OTD measurement range over 10 μs, the modulation frequency of 3.00005 GHz, 3.005 GHz, and 3.05 GHz should also be measured as the above process. Then the unambiguous OTD can be recovered by a traditional and simple phase unwrapping algorithm.

B. Enhancement of SNR and Sensitivity

In the coherent system, the SNR of the received signal can be improved by increasing the power of the LO portion in theory. For PDR technology, the enhancement of SNR would improve the precision of phase detection. For quantitative analysis, we

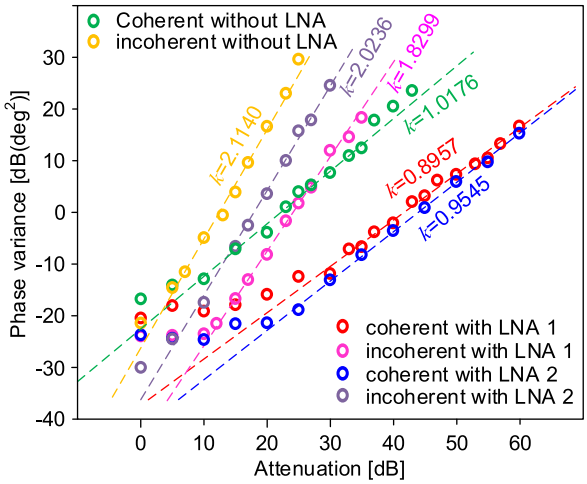

Fig. 6. Verification experiment of SNR improvement. OLUT attenuation versus the phase variance. k is the slope of the fitted straight line. LNA, low noise amplifier.

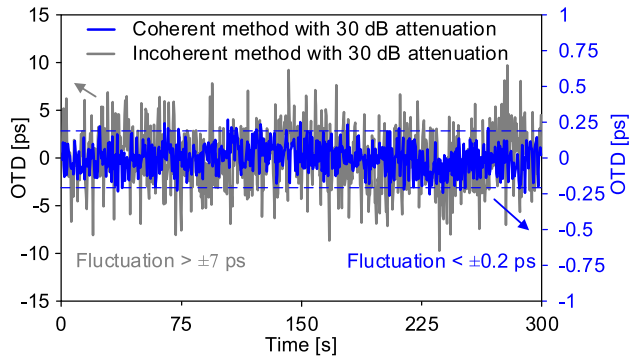

Fig. 7. The system stability of the coherent and incoherent system with an attenuation of 30 dB over 300 seconds. Blue line: Measured OTD under coherent detection; gray line: Measured OTD under incoherent detection.

establish a simple mathematical model. In digital phase detection, the theory Cramer-Rao lower bound (CRLB) can be written as [20]:

$$\mathrm{var}\,(\hat{\varphi}) \geq \frac{1}{N \cdot SNR} \tag{19}$$

where var(.) represents the variance of the measurement parameter, N is the sampling number, SNR is the SNR of the detected signal.

In the coherent detection system, assuming that the power of LO portion is much higher than that in the measurement portion, the thermal noise in PD can be neglected compared to the shot noise. Thus, the SNR can be simplified as follows:

$$SNR_{coherent} \approx \frac{\eta}{2Bq} P_s \tag{20}$$

where P_s is the power of the measurement portion, P_o is the power of the LO portion, B is the bandwidth of the receiver bandwidth, and q is the electron charge.

On the contrary, the incoherent detection often has relatively low power in the receiver, which means thermal noise plays a

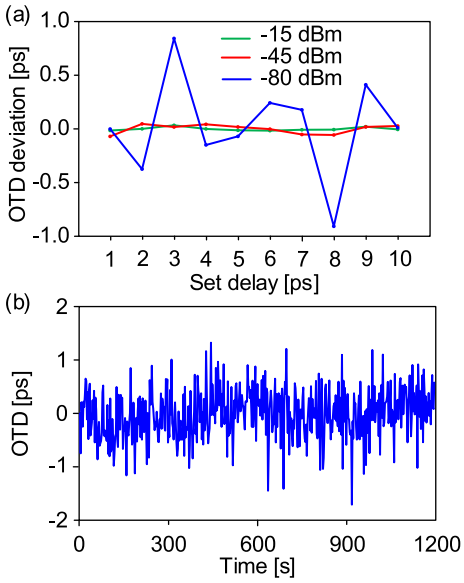

Fig. 8. (a) System accuracy when the power of receiving signal is −15 dBm, −45 dBm, and −80 dBm. (b) System stability when the power of receiving signal is −80 dBm over 1200 s.

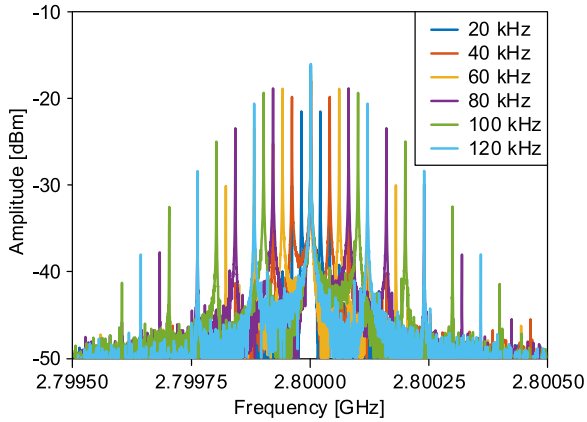

Fig. 9. FFT spectra of the photocurrent when the OLUT is under various vibration frequencies.

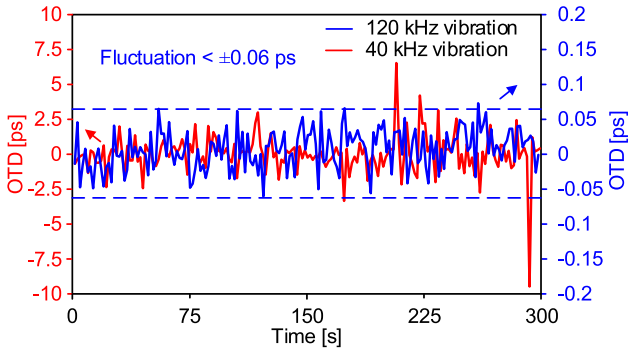

Fig. 10. Measured OTD when the OLUT is under vibration with a 50 kHz IF filter. Blue line: 120 kHz vibration frequency; red line: 40 kHz vibration frequency.

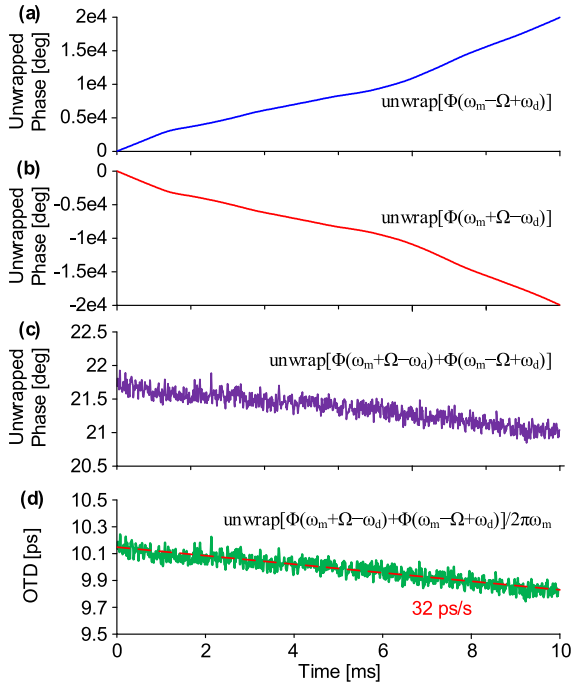

Fig. 11. Results of phase detection by the STFT algorithm over 0.01 seconds when the OLUT is varied with a speed of 32 ps/s. (a) The unwrapped phase of the 2.8 GHz signal. (b) The unwrapped phase of the 3.2 GHz signal. (c) Measured phase after phase variation compensation. (d) Measured OTD after phase variation compensation.

leading role:

$$SNR_{incoherent} \approx \frac{\eta^2 R_L}{4k_b TB} P_s^2 \tag{21}$$

where R_{L} is the load resistance, k_b is the Boltzmann's constant, and T is the absolute temperature.

Combing (19) to (21), the CRLB of the phase discrimination under coherent and incoherent detection can be expressed by:

$$\log\left[\mathrm{var}_{coherent}\left(\hat{\varphi}\right)\right] \geq -\log\left[P_s\right] + \log\left[\frac{2Bq}{N\cdot\eta}\right] \tag{22}$$

$$\log\left[\mathrm{var}_{incoherent}\left(\hat{\varphi}\right)\right] \geq -2\log\left[P_s\right] + \log\left[\frac{4k_b TB}{N\cdot\eta^2}\right] \tag{23}$$

From (22) and (23), the phase variance should be linearly proportional to the power of measurement portion under logarithmic coordinates. With the descent of P_{s}, the variance of phase detection in the incoherent system should have a double descent speed compared with the coherent system. We evaluate the precision improvement of the coherent and incoherent system. A variable optical attenuator (EXFO, FVA-600) is inserted in the OLUT with an attenuation range from 0 dB to 60 dB. The phase variance is calculated with 100 continuous sampling results. The performance of the amplifier is also considered. The gain of LNA1 (RF BAY, LNA-4050) features 25 dB, and the gain of LNA2 (Connphy, CLN-1G18G-3025-S) features 30 dB. As observed in Fig. 6, the slope of the fitted straight line (written as k) fits well with (22) and (23). The additional error may be

TABLE I
COMPARISON OF TYPICAL OTD MEASUREMENT METHODS

Method	Technology	Accuracy	Sensitivity	Doppler effect
Incoherent	Commercial OTDR [22]	3.25 ns	-70 dBm	Immune
	Commercial dispersion analyser [23]	±5 ps*	-40 dBm	Immune
	Commercial PDR [21]	±0.5 ps	-34 dBm	Immune
	Typical PDR method [10]	0.05 ps	-30 dBm	Immune
Coherent	Commercial OFDR [24]	1 ps	-115 dBm	Non-immune
	Typical phase shift method [16]	20 ps*	-72 dBm	Immune
	Proposed work	**±0.08 ps***	**-80 dBm**	**Immune**

* The receiving optical power is less than -40 dBm.

induced by the background noise from the oscilloscope. The coherent system is not sensitive to the signal power compared to the incoherent system under the same amplification gain. It also can be seen that the coherent system provides an absolute advantage in phase detection when the insertion loss of the OLUT is above 15 dB. Thus, based on the results obtained in this study, we can conclude that the SNR of received signal can be enhanced by the coherent PDR method according to theoretical and experimental investigations.

Next, Fig. 7 gives the system OTD fluctuation of the coherent and incoherent systems. It should be noted that environment temperature determines the drift of the OTD while the SNR of the signal determines the fluctuation. The insertion loss of the attenuator is set at 30 dB. During a period of 300 seconds of measurement, the fluctuation of the coherent system is below $\pm$ 0.2 ps while that of the incoherent system is above $\pm$7 ps, indicating the measurement precision is increased by 35 times.

To analyze the system accuracy and sensitivity, we take a motorized variable ODL (General Photonics MDL-002) with an accuracy of $\pm$10 fs to verify the accuracy of the proposed OTD measurement system. The ODL is swept from 1 ps to 10 ps with an interval of 1 ps. As illustrated in Fig. 8(a), the measured OTD deviation from the set value is within $\pm$0.04 ps when the receiving power is -15 dBm. When the receiving power is reduced to $-$45 dBm, the deviation is increased to $\pm$0.08 ps. With a low receiving power of $-$80 dBm, the accuracy of the measurement system is still better than $\pm$0.9 ps. We also test the system stability when the receiving power is $-$80 dBm. In Fig. 8(b), the system fluctuation is within $\pm$1.8 ps. In the experiment, it shows the measurement sensitivity of the system reaches at least $-$80 dBm, which is 46 dB higher than that of commercial PDR products [21]. What's more, the sensitivity can be further increased by using a 14-bit digitizer and lock-in amplifier.

C. Dynamic Measurement

To explore the influence of dynamic measurement in the proposed coherent OTD measurement system, two experiments are carried out respectively. For vibration sensing, the optical fiber with a length of 3 m is wrapped around a piezoelectric ceramic. Due to the piezoelectric effect, the wrapped optical fiber is vibrated with the applied voltage on the piezoelectric ceramic. The frequency of the applied voltage is set from 20 kHz to 120 kHz with an interval of 20 kHz. The FFT spectra of the optical current around 2.8 GHz are shown in Fig. 9, which fits well with the theoretical analysis in (24). In the experiment, the window function width is set as 20 μs, corresponding to an IF bandwidth of 50 kHz. Fig. 10 shows the measured OTD of the fiber with a duration time of 300 s, in which the blue and red lines represent the measured OTD under 120 kHz and 40 kHz vibration. When the vibrating frequency is below the IF bandwidth, the modulated frequency components are leaked into the 2.8 GHz and 3.2 GHz. Vector superposition of the received signal and modulated signal affects the phase detection result. When the vibration frequency is 120 kHz, the OTD fluctuation is below $\pm$0.06 ps. In comparison, for the 40 kHz vibration frequency, the OTD fluctuation deteriorates to $\pm$5 ps. It implies that the proposed coherent system can eliminate the high-frequency vibration effect with a narrower IF filter in the receiver. It should be noticed that the IF filter bandwidth can be narrower by directly increasing the window function width. However, a larger window function width would consume additional time resources, which should be carefully considered based on the specific measurement requirements.

In the low-speed motion experiment, to illustrate the impact of the Doppler effect, a motorized variable ODL is chosen as the OLUT. The sweeping speed of the ODL is set at 32 ps/s first. Considering that the processing time of ADC is much greater than the sweeping time of the ODL (almost several hundred milliseconds), we extract a length of 10 ms signal from the oscilloscope. Short-time Fourier transform (STFT) with a window function width of 16 μs is used to analyze the collected signal, with an overlap percentage of 50%. The phase of ω_{m}–Ω + ω_{d} and ω_{m} + Ω–ω_{d} can be extracted with an interval of 8 μs. The results of phase detection are shown in Fig. 11(a) and (b), respectively, with the unwrapped phase presented to show the impact of the Doppler effect. The total phase shift of the two signals is 19872.4° and -19828.1°, respectively. Since

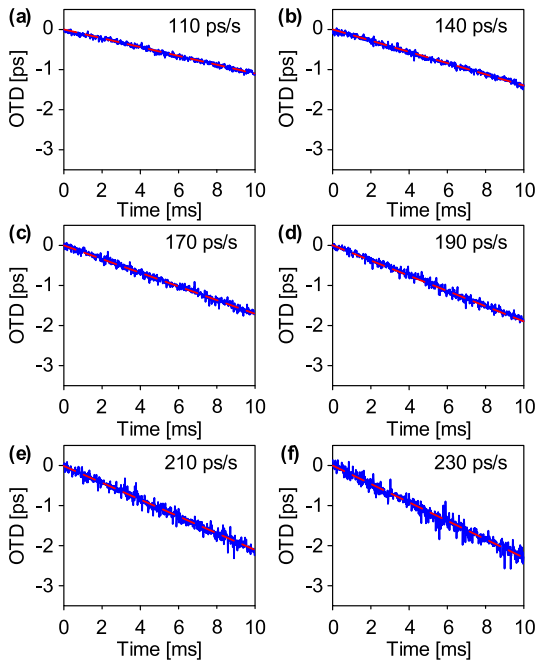

Fig. 12. Measurement OTD of sweeping ODL with a speed of (a) 110 ps/s, (b) 140 ps/s, (c) 170 ps/s, (d) 190 ps/s, (e) 210 ps/s, (f) 230 ps/s.

the sweeping speed is set as 32 ps/s, the doppler frequency can be calculated as 6.128 kHz (i.e., $f_d = vf_c/c = 32$ ps/s $\times 191.5$ THz $/10^{12}$ ps/s). Theoretically, the doppler frequency shift would induce a phase shift of 22060.8° (6.128 kHz $\times 10$ ms $\times 360°$) over 10 ms. Fig. 11(c) shows the results of the measured phase after phase variation compensation, which eliminates both the effect of the Doppler effect and laser phase noise. Finally, Fig. 11(d) gives the measured OTD result, with the dotted line indicating the theoretical change of OTD. Fig. 12 shows the measurement results of ODL at different speeds, including 110 ps/s, 140 ps/s, 170 ps/s, 190 ps/s, 210 ps/s, and 230 ps/s, all of which are consistent with the theoretical values.

IV. Conclusion

Table I gives the performance comparison. The sensitivity of the incoherent systems is usually higher than −40 dBm, except for optical time domain reflectometry (OTDR) [22]. The OTDR-based methods measure OTD by the position of the probe pulse, which means a relatively low SNR is enough for measurement. But it has limited accuracy since a narrow-width pulse is challenging for generation and detection. Other incoherent methods require a high SNR for phase detection to obtain OTD measurement. However, incoherent systems have no advantage in obtaining high SNR when the receiving signal is weak. The coherent systems usually have a higher sensitivity. The optical frequency domain reflectometry (OFDR) [24] method has a sensitivity of −115 dBm but cannot measure variable OTD. The phase shift method [16] eliminates the doppler frequency by applying a quadrature demodulator to achieve the measurement of variable OTD, increasing the system's complexity. Meanwhile, the measurement accuracy of the phase shift method is due to the narrow frequency aperture, usually several MHz. In our system, the frequency aperture is 6 GHz, and thus has an almost 10^3 times accuracy improvement. Moreover, by furtherly optimizing the receiver, the sensitivity of the proposed system has the potential to reach the sensitivity of commercial OFDR products.

In conclusion, we demonstrated an optical PDR method based on coherent detection and demodulation to improve the OTD measurement sensitivity. The effectiveness of removing the laser noise and doppler error has been presented. Theoretical analysis and experimental verification indicated that the coherent optical PDR improves the measurement SNR compared to the traditional incoherent PDR. In the experiment, for the static measurement, a measurement accuracy of ±0.08 ps and a system fluctuation of ±0.2 ps was obtained with an attenuation of 30 dB. The system measurement sensitivity reaches −80 dBm, which is 46 dB better than the commercial PDR products. For the dynamic measurement, with a narrow band IF filter, the effect of high-frequency vibration can be eliminated. In addition, the relative motion of OLUT would not induce extra measurement error. The proposed coherent optical PDR system would have the potential for the application of integrated photonic chips, outdoor free-space optics, LiDAR systems, and fiber-optic sensing networks.

References

[1] X. Ye, F. Zhang, and S. Pan, "Optical true time delay unit for multi-beamforming," *Opt. Exp.*, vol. 23, no. 8, pp. 10002–10008, 2015.
[2] J. Sancho et al., "Integrable microwave filter based on a photonic crystal delay line," *Nature Commun.*, vol. 3, no. 1, pp. 1–9, 2012.
[3] F. Xia, L. Sekaric, and Y. Vlasov, "Ultracompact optical buffers on a silicon chip," *Nature Photon.*, vol. 1, no. 1, pp. 65–71, 2007.
[4] Y. Wang et al., "On-chip optical true time delay lines based on subwavelength grating waveguides," *Opt. Lett.*, vol. 46, no. 6, pp. 1405–1408, 2021.
[5] L. Song, H. Li, and D. Dai, "Mach–Zehnder silicon-photonic switch with low random phase errors," *Opt. Lett.*, vol. 46, no. 1, pp. 78–81, 2021.
[6] X. Wang, Y. Zhao, Y. Ding, S. Xiao, and J. Dong, "Tunable optical delay line based on integrated grating-assisted contradirectional couplers," *Photon. Res.*, vol. 6, no. 9, pp. 880–886, 2018.
[7] X. Wang et al., "Continuously tunable ultra-thin silicon waveguide optical delay line," *Optica*, vol. 4, no. 5, pp. 507–515, 2017.
[8] S. Hong, L. Zhang, Y. Wang, M. Zhang, Y. Xie, and D. Dai, "Ultralow-loss compact silicon photonic waveguide spirals and delay lines," *Photon. Res.*, vol. 10, no. 1, pp. 1–7, 2022.
[9] H. Sun, Y. Wang, and L. R. Chen, "Integrated discretely tunable optical delay line based on step-chirped subwavelength grating waveguide Bragg gratings," *J. Lightw. Technol.*, vol. 38, no. 19, pp. 5551–5560, Oct. 2020.
[10] S. Li, T. Qing, J. Fu, X. Wang, and S. Pan, "High-accuracy and fast measurement of optical transfer delay," *IEEE Trans. Instrum. Meas.*, vol. 70, 2021, Art. no. 8000204.
[11] S. Yokoyama, A. Okamoto, T. Araki, and N. Suzuki, "Examination to eliminate undesirable phase delay of an avalanche photodiode (APD) for intensity-modulated light," *Rev. Sci. Instrum.*, vol. 66, no. 11, pp. 5331–5336, 1995.
[12] T. Qing et al., "High-resolution optical vector analysis with enhanced sensitivity," *IEEE Photon. Technol. Lett.*, vol. 33, no. 11, pp. 581–584, Jun. 2021.
[13] W. Liang, A. Yariv, A. Kewitsch, and G. Rakuljic, "Coherent combining of the output of two semiconductor lasers using optical phase-lock loops," *Opt. Lett.*, vol. 32, no. 4, pp. 370–372, 2007.

[14] S. Camatel and V. Ferrero, "Homodyne coherent detection of ASK and PSK signals performed by a subcarrier optical phase-locked loop," *IEEE Photon. Technol. Lett.*, vol. 18, no. 1, pp. 142–144, Jan. 2006.
[15] J. T. Spollard, L. E. Roberts, C. S. Sambridge, K. McKenzie, and D. A. Shaddock, "Mitigation of phase noise and Doppler-induced frequency offsets in coherent random amplitude modulated continuous-wave LiDAR," *Opt. Exp.*, vol. 29, no. 6, pp. 9060–9083, 2021.
[16] L. Zhou, H. He, J. Sun, and B. Lin, "Phase-shift laser ranging technology based on multi-frequency carrier phase modulation," *Photonics*, vol. 9, no. 9, 2022, Art. no. 603.
[17] F. Fang et al., "Random phase compensation method of coherent LiDAR based on symmetrical double harmonic signals," *Opt. Commun.*, vol. 529, 2023, Art. no. 129003.
[18] S. Banzhaf and C. Waldschmidt, "Phase-code-based modulation for coherent LiDAR," *IEEE Trans. Veh. Technol.*, vol. 70, no. 10, pp. 9886–9897, Oct. 2021.
[19] Z. Xu, F. Yu, B. Qiu, Y. Zhang, Y. Xiang, and S. Pan, "Coherent random-modulated continuous-wave LiDAR based on phase-coded subcarrier modulation," *Photonics*, vol. 8, no. 11, 2021, Art. no. 475.
[20] D. Rife and R. Boorstyn, "Single tone parameter estimation from discrete-time observations," *IEEE Trans. Inf. Theory*, vol. 20, no. 5, pp. 591–598, Sep. 1974.
[21] Suzhou LiuYaoSi, "ODM-C," 2018. [Online]. Available: http://www.newkeytech.com/en/High-precision-Optical-Delay-Meter-PG7042537
[22] Yokogawa, "AQ2780V OPM," 2020. [Online]. Available: http://www.yokogawa.com/pdf/provide/E/GW/Bulletin/0000028710/0/BUAQ7280-01EN.pdf
[23] Agilent, "Agilent86038A," 2004. [Online]. Available: https://www.keysight.com/us/en/assets/9018-02008/user-manuals/9018-02008.pdf
[24] LUNA, "OBR-4600," 2013. [Online]. Available: https://lunainc.com/sites/default/files/assets/files/resource-library/LUNA-Data-Sheet-OBR-4600-V2.pdf